Available online at www.sciencedirect.com
ScienceDirect
Tetrahedron: Asymmetry
Tetrahedron: *Asymmetry* 18 (2007) 260–264

Optical resolution of *N*-formylphenylalanine succeeds by crystal growth rate differences of diastereomeric salts

Laura Bereczki,[a,*] Emese Pálovics,[b] Petra Bombicz,[c] György Pokol,[a] Elemér Fogassy[b] and Katalin Marthi[d]

[a]*Institute of General and Analytical Chemistry, Budapest University of Technology and Economics, H-1521 Budapest, PO Box 91, Hungary*
[b]*Department of Organic Chemical Technology, Budapest University of Technology and Economics, H-1521 Budapest, PO Box 91, Hungary*
[c]*Institute of Structural Chemistry, Chemical Research Center, Hungarian Academy of Sciences, H-1521 Budapest, PO Box 17, Hungary*
[d]*Research Group of Technical Analytical Chemistry, Hungarian Academy of Sciences, Budapest University of Technology and Economics, H-1521 Budapest, PO Box 91, Hungary*

Received 13 December 2006; accepted 25 January 2007

Abstract—Optical resolution of racemic-phenylalanine through its *N*-formyl derivative with a 1-phenylethylamine resolving agent is an effective procedure. Differential scanning calorimetry, single crystal X-ray diffraction and optical microscopy were used in the investigation of the resolution process. It was found that the thermodynamic properties of the given system would not allow the efficient enantiomer separation. Kinetic effects during the crystal formation have been discovered by the comparison of the crystal morphologies of the two diastereomers. The crystal structure of the less soluble diastereomer (*S*)-(−)-1-phenylethylammonium (*S*)-(+)-*N*-formylphenylalaninate salt has been determined and discussed.

1. Introduction

A classical approach tends to treat optical resolution via diastereomeric salt formation as a thermodynamically controlled process. The thermodynamic approach was, in several cases, proven to be an incomplete view of the phenomenon. A characteristic example for the appearance of kinetic effects is the Dutch resolution, when the nucleation inhibition of the simultaneously applied resolving agents[1,2] can be exploited to provide improved enantiomer separation compared to the thermodynamic potentials of the process. Beyond this particular resolution method, in some instances, the outcome of classical resolution processes is determined by the time left for crystallization.[3,4] In these cases, the effect is quite similar to that caused by the change in reaction time and conditions in kinetically controlled organic reactions.

Herein, we report a novel example for the appearance of kinetic control in optical resolutions by diastereomeric salt formation. The optical resolution of phenylalanine through its *N*-formyl derivative **1** by 1-phenylethylamine **2** resolving agent (Fig. 1) is known from the literature,[5] the enantiomer separation is carried out with high efficiency.

Investigation of the thermodynamic background of the process resulted in the realization that the thermodynamic relations of the given system do not make the effective optical resolution possible. Kinetic effects during the crystallization were found to have an important role in the enantiomer separation. Kinetic differences in the formation of the crystalline phases give the determinant contribution to the potential of the resolution process, as previously suggested by Leclerq and Jacques.[6]

2. Results and discussion

2.1. Binary melting phase diagram of the (*S*)-(−)-1-phenylethylammonium (*S*)-(+)- and (*R*)-(−)-*N*-formylphenylalaninate diastereomeric salt pair

The efficiency of the optical resolution of *N*-formylphenylalanine **1** by (*S*)-1-phenylethylamine (*S*)-**2** (Fig. 1) is high,

* Corresponding author. Tel.: +36 1 463 40 65; fax: +36 1 463 34 08; e-mail: lbereczki@mail.bme.hu

0957-4166/$ - see front matter © 2007 Elsevier Ltd. All rights reserved.
doi:10.1016/j.tetasy.2007.01.029

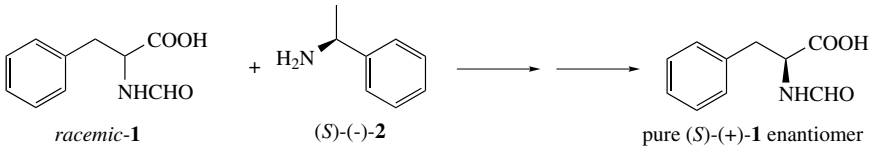

Figure 1. Optical resolution of *N*-formylphenylalanine by an (*S*)-(−)-1-phenylethylamine resolving agent.

the attainable enantiomeric excess is 98%,[5] and the yield is 45%[5] for the (*S*)-**2**–(*S*)-**1** diastereomer.

The melting points and enthalpies of the two diastereomers formed during the resolution process have been determined by the DSC (differential scanning calorimetry) method. 433.7 K and 48.3 kJ/mol were obtained for (*S*)-**2**–(*R*)-**1**, and 436.3 K and 53.6 kJ/mol for (*S*)-**2**–(*S*)-**1**. The differences between the thermoanalytical data of the two diastereomers are small (the differences in the melting points and enthalpies are 2.8 K and 5.3 kJ/mol). Using the DSC results, the solid-melt phase diagram of the two diastereomers was constructed (Fig. 2) and the expected efficiency estimated.[7,8] The melting phase diagram of the system investigated is almost symmetric (eutectic composition: $x_{eu} = 0.54$, eutectic temperature: $T_{eu} = 417.3$ K). According to this, the attainable maximum calculated efficiency of the enantiomer separation[†],[8] would be low (0.148). However, the efficiency on the basis of the experimental results[‡],[8] in the literature[5] is high (0.441).

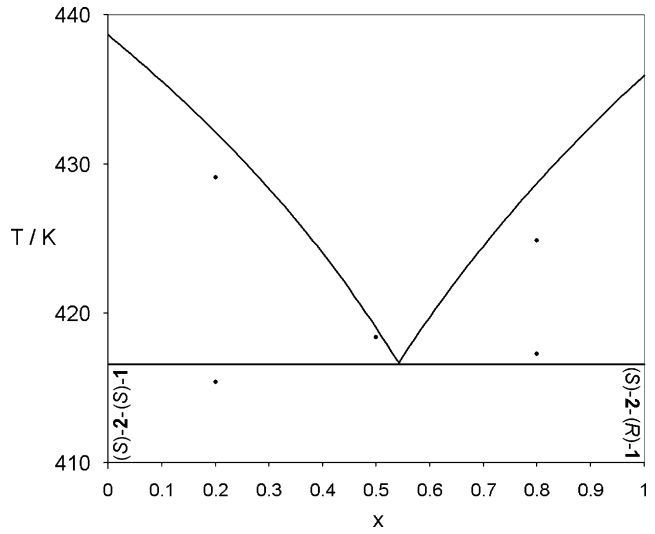

Figure 2. Calculated solid–liquid phase diagram of (*S*)-(−)-1-phenylethylammonium (*S*)-(+)- and (*R*)-(−)-*N*-formylphenylalaninate [(*S*)-**2**–(*S*)-**1** and -(*R*)-**1**] diastereomeric salt pair and measured control points.

2.2. Kinetic aspects in the resolution process

A direct consequence of the near symmetrical binary phase diagram is that the high efficiency of the resolution experiment cannot be explained solely on the basis of thermodynamic considerations. The binary and ternary solubility equilibria of a given diastereomeric system are closely related,[7,8] the chiral recognition processes during the resolution are directly determined by the distribution of the diastereomers between the solid and liquid phases. It was assumed that the kinetic effects became significant in the present case during phase separation. In our search of an explanation for our results, we investigated the resolution process as a function of the time left for crystallization. We found that in a hermetically closed vessel after one week, the enantiomeric excess of the product decreased from 91.9% to 64.9% while the yield increased from 45.0% to 58.2% (*S* decreased from 0.414 to 0.378). When more time was left for the crystallization the more soluble diastereomer (*S*)-**2**–(*R*)-**1** would precipitate together with (*S*)-**2**–(*S*)-**1**, the solution was supersaturated also for the less soluble diastereomer. The amount of (*S*)-**2**–(*R*)-**1** in the solid phase increased five-fold in one week, while the amount of the less soluble salt only increased slightly (with ca. 10%).

An explanation can be given to the initially high experimental yield considering that the starting concentration of the solution used in the resolution experiment was quite high, it got in the range where the solution was saturated for both diastereomers. In this concentration interval both diastereomers should precipitate, resulting in decreased enantiomeric excess. However, with prompt workup only (*S*)-**2**–(*S*)-**1** was present in the crystalline phase with high selectivity, the enantiomeric excess was high. We assume that the formation of (*S*)-**2**–(*S*)-**1** crystalline phase has a remarkable kinetic advantage over (*S*)-**2**–(*R*)-**1**, the crystal growth rate of (*S*)-**2**–(*S*)-**1** notably exceeds that of its diastereomer. When the reaction mixture is worked up immediately, (*S*)-**2**–(*R*)-**1** remains in the mother liquor notwithstanding that the solution is saturated for both diastereomers.

Investigation of the crystal morphology of the two diastereomers (Figs. 3a and 3b) gives a greater insight into the kinetics of the process. Crystals of the two diastereomers were prepared from enantiomerically pure acid and base under similar crystallization conditions. Both diastereomers gave needle-like crystals, however, a large difference was observed in the crystal growth rate of the diastereomers in perpendicular directions to the longitudinal direction of the crystals. While (*S*)-**2**–(*S*)-**1** crystallized as large single crystals, (*S*)-**2**–(*R*)-**1** formed thin thread-like crystals, the crystal growth of the latter being strongly inhibited in transversal directions. Figures 3a and 3b show a clear picture of the difference in crystal morphology in the case of the two diastereomers.

[†] $S = \frac{2x_{eu}-1}{x_{eu}}$.
[‡] Efficiency = yield·enantiomeric excess.

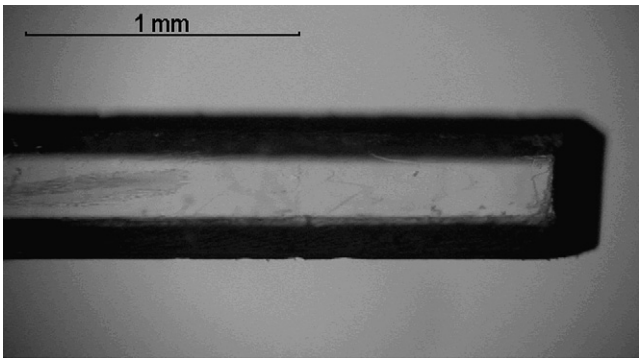

Figure 3a. Crystal morphology of the less soluble (*S*)-**2**–(*S*)-**1** diastereomer.

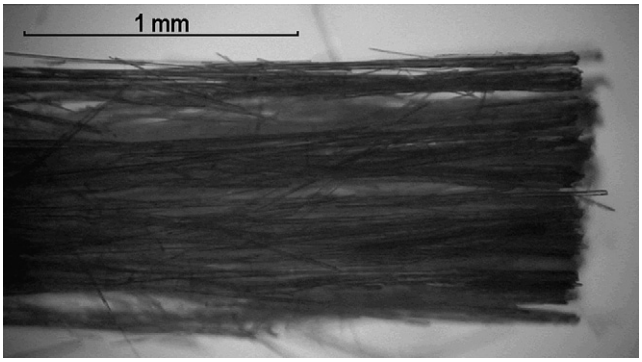

Figure 3b. Crystal morphology of the more soluble (*S*)-**2**–(*R*)-**1** diastereomer.

2.3. Molecular and crystal structure (*S*)-(−)-1-phenylethylammonium (*S*)-(+)-*N*-formylphenylalaninate

One cation and one anion of the salt can be found in the asymmetric unit (Fig. 4) of (*S*)-(−)-1-phenylethylammonium (*S*)-(+)-*N*-formylphenylalaninate (*S*)-**2**–(*S*)-**1**.

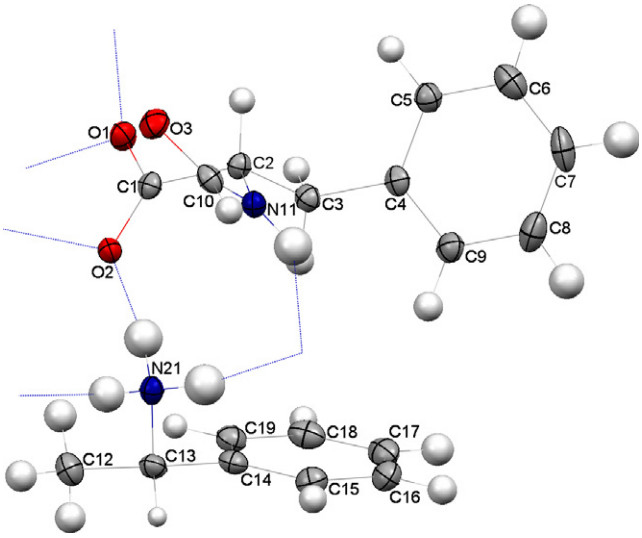

Figure 4. The ORTEP[9] diagram of the salt (*S*)-**2**–(*S*)-**1** shows the content of the asymmetric unit at 50% probability level. N–H···O type intermolecular interactions are drawn by dotted line.

Figure 5 shows the solid-state molecular and crystal packing arrangement determined by single crystal X-ray diffraction of (*S*)-(−)-1-phenylethylammonium (*S*)-(+)-*N*-formylphenylalaninate (*S*)-**2**–(*S*)-**1** salt.

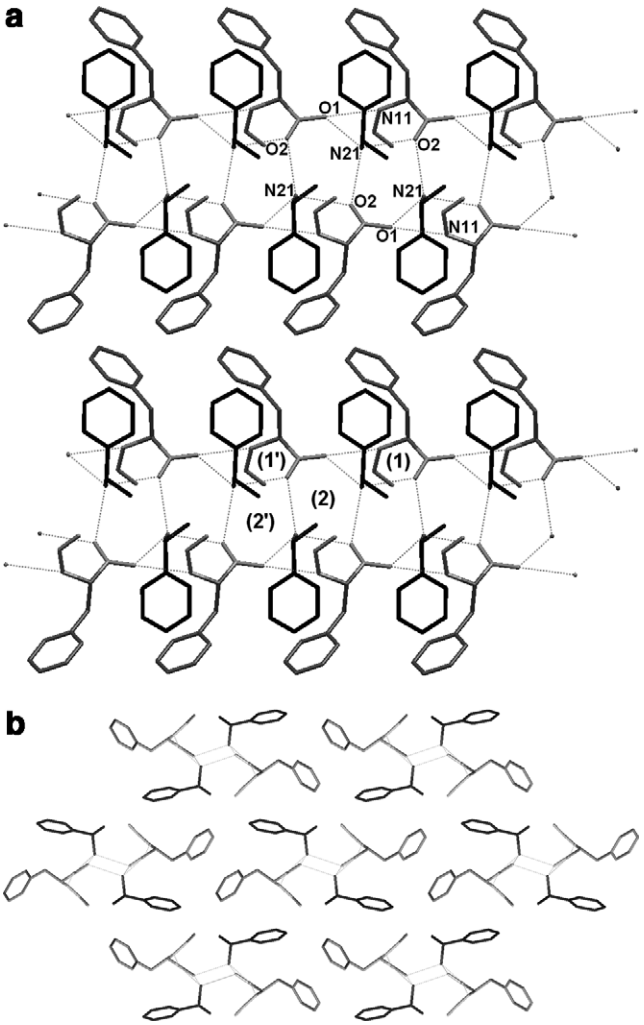

Figure 5. (a) The infinite inner hydrophilic, outer hydrophobic column organized along the 2_1 axis in the direction of the 'a' crystallographic axis in the crystal structure of (*S*)-**2**–(*S*)-**1**.[9] The hydrogen bond loops of the extensive hydrogen bond system are indicated with numbers in the middle of the column. (b) Placement of the outer hydrophobic columns in the crystal structure viewed along the 'a' crystallographic axis.

In the crystal of (*S*)-**2**–(*S*)-**1** the organic cations and anions are arranged in columns. There is an infinite column in the 'a' crystallographic direction along the twofold screw (2_1) axis. These columns are hydrophilic inside and hydrophobic outside. An extended strong N–H···O type hydrogen bond system organizes the column[10] (Table 1). Two cations and two anions form a 'turn' of the column (Fig. 5a). The N–H···O hydrogen bonds form two loops: loop (1) on the side of the hydrogen bond system connecting one cation and two anions is $R_3^2(9)$, while (2) in the core connecting two cations and two anions is $R_4^3(10)$ by the graph set descriptor.[11–13] Three of the four N–H···O hydrogen bonds are parts of two loops: N21–H21B···O2 and N21–H21A···O1 can be found in both (1) and (2), respectively,

Table 1. Intermolecular interactions in the crystal structure of (*S*)-(−)-1-phenylethylammonium (*S*)-(+)-*N*-formylphenylalaninate (*S*)-**2**–(*S*)-**1**

D–H···A	D–H [Å]	H···A [Å]	D···A [Å]	D–H···A [Å]	Symm. op.	Loop
N11–H11···O1	0.91(2)	2.16(2)	2.862(2)	134(2)	$1+x, y, z$	1
N21–H21A···O1	0.98(2)	1.82(2)	2.782(2)	169(2)	$1+x, y, z$	1&2
N21–H21B···O2	0.98(2)	1.80(2)	2.767(2)	170(2)		1&2
N21–H21C···O2	0.93(2)	1.93(2)	2.857(2)	175(2)	$1/2+x, 1/2-y, 1-z$	2&2′
C10–H10···O1	1.02(2)	2.55(2)	3.106(2)	114(1)	$1+x, y, z$	1
C12–H12C···O3	0.99(2)	2.57(2)	3.164(2)	119(1)	$1/2+x, 1/2-y, 1-z$	
C13–H13···O3	1.00(2)	2.54(2)	3.215(2)	125(1)	$1/2+x, 1/2-y, 1-z$	
C18–H18···O3	0.96(2)	2.53(2)	3.440(2)	158(1)	$1/2-x, -y, 1/2+z$	

furthermore N21–H21C···O2 takes part in two connecting (2) and (2′) rings. O3 is ill placed for a strong hydrogen bond, as well as forming weak C–H···O type interactions within the column with C12–H12C and C13–H13, while the only intercolumn hydrogen bond keeping the columns together is the weak C18–H18···O3 interaction (Fig. 5b).

This unique hydrogen bond system constructing the column and keeping the columns parallel by hydrogen bonds can only be realized by this particular configuration of the organic ions, which explains the capability of the diastereomer separation. The placement of the O3 atom is determined by the chirality of C2 in (*S*)-**1**. O3 takes part in the intercolumn hydrogen bond in (*S*)-**2**–(*S*)-**1** but there may be hindrance of O3 hydrogen bond formation, thus causing transversal crystal growth because of the different chirality of C2 in (*S*)-**2**–(*R*)-**1** resulting in enhanced optical resolution by diastereomeric salt formation.

Single crystals grown from (*S*)-**2**–(*R*)-**1** were not suitable for X-ray diffraction studies since their transversal dimensions were about 0.01 mm. The crystal growth of (*S*)-**2**–(*R*)-**1** is kinetically inhibited in transversal directions.

We have verified that the powder diffractogram measured of the (*S*)-**2**–(*S*)-**1** sample used for the thermal investigations was in agreement with that generated from the single crystal X-ray data.

3. Conclusion

Optical resolution by diastereomeric salt formation is generally considered as a thermodynamically controlled process since kinetic effects are rarely determining factors. In the presented example however, the great difference in the crystal growth kinetics of the diastereomers made successful optical resolution possible. In this case, thermoanalytical data turned our attention towards the kinetic aspects of the process.

Selective crystallization of one diastereomer in the resolution experiment is due to the larger stability of its crystalline phase under the given conditions. It can be observed in the presented example that apart from influencing the thermodynamic stability of the diastereomeric structures, the efficiency of the resolution can be improved also by exploiting kinetic potentials. The presented unique structure that was made up of inner hydrophilic, outer hydrophobic columns was ideal to let kinetic effects be expressed, since the junction of the molecular columns that is strongly dependent on weaker second order interactions determined the rate of crystal growth. Thermodynamic differences between the diastereomeric structures were small, whereas the kinetic differences quite expressed, that allowed an estimate of the importance of a possible crystal growth kinetic effect in an optical resolution via diastereomeric salt formation. This effect was found to have significant practical importance from the point of view of the resolution efficiency.

4. Experimental

4.1. Materials and methods

The chemicals used in this paper were purchased from Aldrich. Optical rotations were determined on a Perkin–Elmer 241 polarimeter. X-ray powder diffractograms were taken on a Freiburger Prazisionsmechanik (Carl Zeiss) HZG4 X-ray diffractometer. The measurements were carried out in the $2\Theta = 2$–$44°$ range at the CuK_α line at room temperature. The accelerator voltage was 30 kV, the current 25 mA. DSC measurements were performed with TA Instruments DSC 2920. Visual investigations were carried out by a Leica MZ6 polarizing microscope. The crystallization processes were recorded with a JVC GCX3 digital camera.

4.2. Optical resolution of *N*-formylphenylalanine by (*S*)-(−)-1-phenylethylamine (prompt workup)

A mixture of racemic **1** (0.986 g, 5.1 mmol) and (*S*)-(−)-**2** (0.619 g, 5.1 mmol) was dissolved in water (2 cm^3) under heating. The solution was cooled down to room temperature and formation of a crystalline precipitate occurred upon scratching. The crystalline phase was filtered off and washed with water (2×0.5 cm^3) to give 0.313 g of crystalline product (19.5%), which was dissolved in water (0.6 cm^3) under heating. Concentrated HCl (0.6 cm^3) was then added and the solution cooled down in a refrigerator. After 2 h it was filtered and washed with water (3×0.5 cm^3). The process yielded 0.222 g (*S*)-(+)-**1**, $[\alpha]_D^{20} = +69.1$ (*c* 2, ethanol), ($[\alpha]_D^{20}$ (100%) = +75.2).[5]

4.3. Optical resolution of *N*-formylphenylalanine by (*S*)-(−)-1-phenylethylamine (workup after one week)

A mixture of racemic **1** (0.982 g, 5.1 mmol) and (*S*)-(−)-**2** (0.616 g, 5.1 mmol) was dissolved in water (2 cm^3) under

heating. The crystallization was started by scraping the recipient with a glass stick. The solution was cooled down and left at room temperature for one week. The crystalline phase was filtered out and washed with water (2×0.5 cm^3) to give 0.417 g of a crystalline product (26.1%). This was dissolved in water (0.6 cm^3) under heating after which cc. HCl (0.6 cm^3) was added, and the solution cooled down in a refrigerator. After 1 h, the solution was filtered and washed with water (3×0.5 cm^3). The process yielded 0.286 g (*S*)-(+)-**1**, $[\alpha]_D^{20} = +48.8$ (*c* 2, ethanol).

4.4. X-ray crystallography

Single crystals of (*S*)-**1**–(*S*)-**2** were gained by salt formation from (*S*)-(−)-1-phenylethylamine and (*S*)-(+)-*N*-formylphenylalanine in water. A crystal of (*S*)-**2**–(*S*)-**1** salt was mounted on a loop.

Cell parameters were determined by least-squares of the setting angles of 2693 reflections. Empirical formula: $C_{10}H_{10}NO_3^-C_8H_{12}N^+$, formula weight: 314.38, colourless, needle crystals, size: $0.40 \times 0.20 \times 0.20$ mm, crystal system: orthorombic, space group $P2_12_12_1$, unit cell dimensions: $a = 6.1105(4)$ Å, $b = 16.2543(8)$ Å, $c = 16.8035(8)$ Å, $V = 1668.9(2)$ Å^3, $T = 93(2)$ K, $Z = 4$, $F(000) = 672$, $D_x = 1.253$ g/cm^3, $\mu = 0.694$ mm^{-1}.

Intensity data were collected on a Rigaku R-AXIS RAPID image plate diffractometer (graphite monochromator; CuKα radiation, $\lambda = 1.54180$ Å) at 93(2) K in the range $2.6316 \leqslant \theta \leqslant 72.1250°$. A total of 22952 reflections were collected of which 2964 were unique ($R(\text{int}) = 0.030$).

The initial structure model was obtained by direct methods[14] and subsequent difference synthesis. Numerical absorption correction was performed ($T_{\min} = 0.853$, $T_{\max} = 0.922$). Anisotropic full-matrix least-squares refinement[15] on F^2 for all non-hydrogen atoms yielded $R_1 = 0.0303$ and $wR_2 = 0.0607$ for 2762 [$I > 2\sigma(I)$] and $R_1 = 0.0345$ and $wR_2 = 0.0627$ for all intensity data (number of parameters = 297, goodness-of-fit = 1.176, absolute structure parameter $x = -0.2(2)$). This organic salt does not contain a centre, which has significant anomalous X-ray dispersion. Therefore, the absolute structure parameter[16] as determined by single crystal diffraction has large esd. Crystals were prepared from enantiomerically pure starting compounds. The configuration of the single crystal structure is in agreement with the known absolute structure.

The maximum and mean shift/esd is 0.000 and 0.000. The maximum and minimum residual electron density in the final difference map was 0.15 and −0.15 e/Å^3. The applied weighting scheme was $w = 1/[\sigma^2(F_o^2) + (0.0179P)^2 + 0.4161P]$ where $P = (F_o^2 + 2F_c^2)/3$. Hydrogen atomic positions were found on the difference Fourier maps.

Crystallographic data (excluding structure factors) for the above crystal structure have been deposited with the Cambridge Crystallographic Data Centre as supplementary publication number CCDC 627510.

Acknowledgements

The Hungarian OTKA Foundation (Project Nos. T042725, F037814 and T042642) and a diffractometer purchase grant from the National Office for Research and Technology (MU-00338/2003) are gratefully acknowledged for financial support.

References

1. Nieuwenhuijzen, J. W.; Grimbergen, R. F. P.; Koopman, C.; Kellogg, R. M.; Vries, T. R.; Pouwer, K.; van Echten, E.; Kaptein, B.; Hulshof, L. A.; Broxterman, Q. B. *Angew. Chem., Int. Ed.* **2002**, *41*, 4281–4286.
2. Dalmolen, J.; Tiemersma-Wegman, T. D.; Nieuwenhuijzen, J. W.; van der Sluis, M.; van Echten, E.; Vries, T. R.; Kaptein, B.; Broxterman, Q. B.; Kellogg, R. M. *Chem. Eur. J.* **2005**, *11*, 5619–5624.
3. Kozma, D.; Novák, C.; Pokol, G.; Fogassy, E. *J. Therm. Anal.* **1996**, *47*, 727–733.
4. Bálint, J.; Egri, G.; Kiss, V.; Gajáry, A.; Juvancz, Z.; Fogassy, E. *Tetrahedron: Asymmetry* **2001**, *12*, 3435–3439.
5. Overby, L. R.; Ingersoll, A. W. *J. Am. Chem. Soc.* **1951**, *73*, 3363–3366.
6. Leclerq, M.; Jacques, J. *Bull. Soc. Chim. Fr.* **1975**, 2052–2056.
7. Jacques, J.; Collet, A.; Wilen, S. H. *Enantiomers, Racemates, and Resolutions*; Krieger Publishing Company: Malabar, Florida, 1981.
8. Kozma, D.; Pokol, G.; Ács, M. *J. Chem. Soc., Perkin Trans. 2* **1992**, 435–439.
9. Macrae, C. F.; Edgington, P. R.; McCabe, P.; Pidcock, E.; Shields, G. P.; Taylor, R.; Towler, M.; van De Streek, J. *J. Appl. Crystallogr.* **2006**, *39*, 453–457.
10. Vandersluis, P.; Spek, A. L. *Acta Crystallogr., Sect. A* **1990**, *46*, 194–201.
11. Etter, M. C. *Acc. Chem. Res.* **1990**, *23*, 120–126.
12. Bernstein, J.; Davis, R. E.; Shimoni, L.; Chang, N.-L. *Angew. Chem., Int. Ed.* **1995**, *34*, 1555–1573.
13. Grell, J.; Bernstein, J.; Tinhofer, G. *Acta Crystallogr., Sect. B: Struct. Sci.* **1999**, *55*, 1030–1043.
14. Altomare, A.; Cascarano, G.; Giacovazzo, C.; Guagliardi, A. *J. Appl. Crystallogr.* **1993**, *26*, 343–350.
15. Barbour, L. J. *J. Supramol. Chem.* **2001**, *1*, 189–191.
16. Flack, H. D. *Acta Crystallogr., Sect. A* **1983**, *39*, 876–881.